

Robust Analysis of Multi-Task Learning on a Complex Vision System

Dayou Mao¹

daniel.mao@uwaterloo.ca

Yuhao Chen¹

yuhao.chen1@uwaterloo.ca

Yifan Wu¹

yifan.wu1@uwaterloo.ca

Maximilian Gilles²

maximilian.gilles@kit.edu

Alexander Wong¹

a28wong@uwaterloo.ca

¹Vision and Image Processing Research Group, University of Waterloo

²Karlsruhe Institute of Technology (KIT), Karlsruhe, Germany

Abstract

Multi-task learning (MTL) has been widely studied in the past decade. In particular, dozens of optimization algorithms have been proposed for different settings. While each of them claimed improvement when applied to certain models on certain datasets, there is still lack of deep understanding on the performance in complex real-worlds scenarios. We identify the gaps between research and application and make the following 4 contributions. (1) We comprehensively evaluate a large set of existing MTL optimization algorithms on the MetaGraspNet dataset designed for robotic grasping task, which is complex and has high real-world application values, and conclude the best-performing methods. (2) We empirically compare the method performance when applied on feature-level gradients versus parameter-level gradients over a large set of MTL optimization algorithms, and conclude that this feature-level gradients surrogate is reasonable when there are method-specific theoretical guarantee but not generalizable to all methods. (3) We provide insights on the problem of task interference and show that the existing perspectives of gradient angles and relative gradient norms do not precisely reflect the challenges of MTL, as the rankings of the methods based on these two indicators do not align well with those based on the test-set performance. (4) We provide a novel view of the task interference problem from the perspective of the latent space induced by the feature extractor and provide training monitoring results based on feature disentanglement.

1. Introduction

The demand for efficient model architectures that can handle multiple vision tasks simultaneously has given rise to

the concept of Multi-task Learning (MTL). In practical applications, MTL offers a solution to reduce model size, saving time, memory, and potentially reducing power consumption. At its core, MTL networks distribute parameters to extract shared feature representations across various tasks, while employing task-specific heads to decode these shared representations for individual downstream tasks. This architectural approach not only offers computational benefits but also holds the promise of more robust feature extraction as tasks become more complex. By training a model to handle multiple tasks, the backbone network is effectively regularized to learn richer features, potentially leading to improved performance [11, 30, 47, 48, 52, 54, 68]. Notable predecessors in this field encompass OverFeat [56], Fast R-CNN [18], Mask R-CNN [24], and so on.

Despite the myriad advantages that the MTL framework promises, training a multi-task model typically poses more formidable challenges compared to single-task models [1, 24, 31, 65, 76]. This is commonly known as the problem of “negative transfer”. This heightened complexity stems from the diverse range of vision tasks, each with its own unique difficulty levels, output dimensions, and training loss functions. Consequently, it is a rare occurrence for all these tasks to seamlessly align during the training process. Instead, a prevalent issue known as “task interference” frequently manifests, comprising two principal aspects: task conflicts and task imbalance. Task conflicts [20, 55, 66, 76] refer to a scenario in which the act of updating network parameters along the steepest descent direction of the loss function for one task may inadvertently lead to a degradation in the performance of another task. This subtle issue can be discerned by analyzing the angles between the gradients computed for different task losses. Task imbalance [25, 55], on the other hand, pertains to situations where

the learning process of one specific task dominates over the others, causing an uneven distribution of focus among the tasks. This can be identified by evaluating the relative norms of the gradients derived from the various task losses.

Extensive research has delved into MTL techniques aimed at mitigating the issues of task conflicts and task imbalance, as we will elaborate upon in more detail in Section 2. However, we observed the following research gaps: performance benchmark on the robotic grasping domain, proof of validity of feature-level gradients, and comprehensive identification of task interference. (1) The existing literature is mostly focused on toy examples [5, 6, 33, 37–39, 46, 55, 72], Celeb-A [6, 35, 39, 40, 54, 72], CityScapes [30, 35, 38–40, 46, 54, 55, 72], NYU/NYU-v2 [5, 35, 38–40, 46, 55, 59, 72, 73], Multi-MNIST [32, 54, 59, 72], Multi-Fashion-MNIST [37, 38], Multi-Task CIFAR-100 [6, 72], and QM-9 [39, 46]. However, we noticed few experiments done with complex vision tasks across a diverse range of tasks. (2) Many prior works have proposed to use feature-level gradient to replace parameter-level gradient for more efficient computation, but lack theoretical guarantee or solid empirical analysis to prove its effectiveness. (3) Most proposed optimization algorithms claim that there are problems of task conflicts and task dominance and propose to reduce either one or both of these two types of task interference. But there is lack of evidence for their validity in real applications with complex data and a wide range of tasks.

In this paper, we address the aforementioned issues by carrying out comprehensive evaluations of the existing MTL optimization algorithms on the MetaGraspNet dataset [17], as it brings new test ground for multi-task learning due to its real-world application value and complexity. Our contribution is 4-fold:

- we provide benchmark results on MetaGraspNet dataset of a large set of MTL optimization algorithms, answer the question of “whether the existing methods are still applicable to complex real-world settings”, and conclude the best performing methods (Section 3);
- we address the commonly used technique of replacing parameter-level gradients with feature-level gradients and empirically demonstrate that this does not generalize to all methods and has to be analyzed and tested for each (Section 4);
- we provide robust analysis on the phenomenon of task interference, show that comparison between methods based on the train-time task conflicts and task balancing indicators does not align well with those based on test-time performance, and conclude that gradient angles and gradient relative norms cannot clearly reflect the challenges in complex real-world MTL scenario (Section 5);
- we provide a novel view towards the problem of task interference in MTL from the perspective of learning disen-

tangled features for different vision tasks and draw people’s attention to the structure of the latent space induced by the feature extractor (Section 6).

2. Problem Definition and Related Work

The problem of Multi-Task Learning aims to train a model to learn several tasks simultaneously. Formally, we assume for the following notations. T denotes the number of tasks. \mathcal{X} denotes the set of training examples (RGBD images in our case). $\mathcal{Y} = \bigoplus_{i=1}^T \mathcal{Y}_i$ denotes the space of task labels \mathcal{Y}_i . $\mathcal{D} \subset \mathcal{X} \times \mathcal{Y}$ denotes the training dataset. $f_\theta : \mathcal{X} \rightarrow \mathcal{Y}$ denotes a neural network parametrized by $\theta \in \Omega$ where Ω is the parameter space. $\mathcal{L}_i : \mathcal{Y} \times \mathcal{Y} \rightarrow \mathbb{R}$ denotes the loss functions for the i -th task. In general, multi-task learning can be formulated as the following optimization problem:

$$\min_{\theta \in \Omega} \sum_{(x,y) \in \mathcal{D}} \mathcal{L}(f_\theta(x), y), \quad (1)$$

where \mathcal{L} is some loss function, possibly vector-valued, that is defined on $\mathcal{Y} \times \mathcal{Y}$. The vanilla form of this loss function \mathcal{L} is to take the sum of each task losses \mathcal{L}_i , while Pareto optimization [37, 46, 54] is to put all losses as a T -dimensional vector, and minimize the loss vector following the partial-order on \mathbb{R}^T that is induced by the cone \mathbb{R}_+^T .

2.1. Gradient Manipulation

Gradient manipulation methods [6, 13, 35, 38, 46, 54, 55, 66, 72] aim to replace the gradient derived for the vanilla loss (sum or average) by a linear combination of the gradients derived for each loss. Formally, let $d \in \mathbb{N}$ denote the total number of trainable parameters in the model, $g_i := \nabla_\theta \mathcal{L}_i \in \mathbb{R}^d$ denote the gradients derived for the i -th task, $i \in \{1, \dots, T\}$, and $\hat{g} := \sum_{i=1}^T \alpha_i g_i \in \mathbb{R}^d$ denote the final gradient, where $\alpha_i \in \mathbb{R}$ for $i \in \{1, \dots, T\}$. Gradient manipulation methods are algorithmic ways to determine the coefficients $\alpha = (\alpha_1, \dots, \alpha_T)^\top \in \mathbb{R}^T$ based on different heuristics or objectives. Computation of the gradient coefficients can be done both explicitly or implicitly.

Explicit approaches [6, 35, 66, 72] have closed-form formulae, and may rely on some stochasticity. PCGrad [72] proposed to reduce task conflicts by projecting gradients onto the normal planes of each other, whenever the angle between two gradient vectors is obtuse. GradVac [66] expanded along this direction and proposed to constraint the angles to be acute. The lower bound on the cosine values is determined by exponential moving average, with the initial value set to 0, same as PCGrad. GradDrop [6] proposed a concept of Gradient Positive Sign Purity, interpret it as a probability, and mask the positive gradients with this purity and the negative ones with the complement. Random Gradient Weighting (RGW) [35] draws samples from a Gaussian distribution, normalize them into a probability simplex, and directly use these normalized samples as gradient weights.

Another line of research [13, 38, 46, 54, 55] proposes implicit approaches to compute a weighting of the gradients. This could be achieved by solving either an optimization problem or a system of equations. MGDA [54] defines the weights to be such that the weighted sum of the raw gradients is the norm minimizer within the convex hull enclosed by the raw gradients. IT-MTL [13] proposed a measurement of task transference and select the gradient update that would maximize task transference from a pool of candidate gradients at each training iteration. CAGrad [38] proposed to maximize the minimum amount of decrease (in absolute value) in the individual losses. The dual form of this problem resolves to determining the best weighting for the individual gradients, w.r.t. the dual objective. Nash-MTL [46] follows a similar idea as CAGrad, but rather than maximizing the minimum amount of decrease, it maximizes the sum of the log decreases in each individual loss. This eventually resolves to solving a (non-linear) system of equations. Aligned-MTL [55], proposed to approximate the gradient matrix with a unitary matrix, which is sure to have stability number equal 1. This approximation can be computed via a closed form formula based on the spectral decomposition of the Gram matrix, which is positive semi-definite, and the final update direction is simply defined to be the summation of the approximated gradients.

2.2. Gradient Balancing

Similar to gradient manipulation methods reviewed in the previous section, gradient balancing methods [5, 21, 26, 30, 35, 37, 39–41, 73], or task balancing methods, aim to assign weights to the loss functions so that all tasks are learned at the same pace. Formally, this family of algorithms are to find $w = (w_1, \dots, w_T)^\top \in \mathbb{R}_{\geq 0}^T$ and then solve the balanced optimization problem

$$\min_{\theta \in \Omega} \sum_{(x, y) \in \mathcal{D}} \sum_{i=1}^T w_i \mathcal{L}_i(f_\theta(x), y_i) \quad (2)$$

Gradient balancing method can be broadly divided into explicit approaches, implicit approaches, and automatic approaches.

Explicit approaches include [5, 21, 35, 40, 41, 73]. Grad-Norm [5] proposes to control the learning pace of different tasks based on the relative norm of the gradients and does so by assigning task weights and updating them at each training iteration. Guo [21] and Yun [73] proposed different ways to evaluate the performance of each task and re-weigh the losses based on performance. Almost exactly the same as RGW [35], the same paper also proposed Random Loss Weighting (RLW) to randomly assign weights to the task losses. In [41], the authors proposed yet another simple weighting mechanism named Dynamic Weight Average (DWA) to re-weight the losses based on the relative descending rate of each loss.

Implicit approaches [37, 39] compute the weights w by solving an optimization subproblem at each training iteration. Among these, Lin [37] proposed to decompose the Pareto optimization problem into subregions, and propose a different candidate solution per-subregion. Utilizing the work in [14] and the dual problem, Lin formulated the Pareto optimization problem as assigning weights to the individual objectives. On the other hand, FAMO [39] proposed that the parameter update at each training step should maximize the lowest relative improvement of the task losses. The subtle difference from CAGrad [38] is that FAMO uses *relative* improvements, so that solving the optimization subproblem results in reducing gradient dominance, whereas CAGrad uses *absolute* improvements and would result in reducing gradient conflicts.

Finally, automatic approaches [26, 30] dynamically updates the loss weights together with the network parameters by using the optimizer. The main difference between automatic and non-automatic approaches is that the loss weights are treated as trainable parameters in addition to those in the network in automatic approaches, whereas the weights are non-trainable, though dynamic, and manually updated at each iteration.

2.3. Gradient Regularization

Gradient regularized training [9, 19, 27, 57, 64] has a long history. Previous work mainly focuses on penalizing for gradients or Hessians of large norm and claim that models trained with this form of regularization are more robust to adversarial attacks. Applications in the topic of multi-task learning follow the same idea in essence. People again aim to regularize the gradients derived for individual tasks by adding regularization terms to the total loss [28, 59]. Now differently, the goal is to resolve gradient conflicts.

Instead of developing deterministic, stochastic, or optimization-based heuristics as the gradient manipulation and gradient balancing methods, the final update of the network parameters can also be determined automatically during the course of training.

In general, the optimization problem now takes the form

$$\min_{\theta \in \Omega} \sum_{(x, y) \in \mathcal{D}} \mathcal{L}(f_\theta(x), y) + \mathcal{L}_{\text{reg}}(G) \quad (3)$$

where $G := [g_1, \dots, g_T] \in \mathbb{R}^{d \times T}$ is the matrix whose columns are made up of the task gradients $g_i = \nabla_\theta \mathcal{L}_i$.

In particular, Suteu [59] argued that task gradients are better to be orthogonal and added squared cosine similarity as a regularization term. Javaloy [28] proposed to regularize the gradients by minimizing the angles between each task gradient and the average of all task gradients.

We make three remarks here on the differences and relationships between the aforementioned three categories. (1) Due to the linearity of the gradient operator ∇ , scaling the

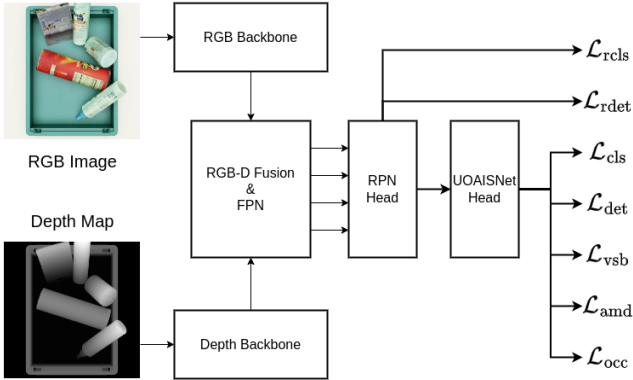


Figure 1. Illustration of network architecture.

loss function and scaling the gradients are essentially the same. However, gradient manipulation methods aim to manipulate the *directions* of the gradients to resolve *task conflicts*, whereas gradient balancing methods aim to manipulate the *magnitudes* of the gradients to resolve *task dominance*. (2) Gradient manipulation methods focus more on manipulating gradients for the shared parameters whereas gradient balancing methods manipulate gradients for all parameters. (3) Wherever the raw gradients $\nabla \mathcal{L}_i$ is needed, regardless of solving task conflicts or task dominance in nature, we can consider both parameter-level gradients $\nabla_{\theta^{\text{sh}}} \mathcal{L}_i$ and feature-level gradients $\nabla_{\mathcal{Z}} \mathcal{L}_i$, where θ^{sh} is the shared parameters and \mathcal{Z} is the shared representation. We provide more investigations on point (3) later in the paper.

2.4. Network Design

We briefly cover the existing research on network architecture design without going into too much details, as this is not the focus of our work. The application of this concept of multi-task learning is also not a recent thing [11, 12, 18, 24, 31, 34, 45, 47, 49, 56, 60, 61]. More advanced designs include feature fusion methods [10, 15, 29, 44, 53, 70], feature selection (attention mechanism) [3, 41, 43], task information distillation [63, 68, 74–76], knowledge distillation [4, 26, 69, 71], and neural architecture search [7, 8, 16, 20, 22, 42, 50, 58, 62].

3. Benchmark on MetaGraspNet Dataset

In this section, we answer the question of “how the existing MTL optimization algorithms perform in complex real-world vision systems and what are the best-performing methods”.

Network Architecture Overview. We follow the work [2] and utilize two ResNets [23], one for RGB image input and one for gray-scaled depth map input. These two ResNets serve as our backbones, outputting feature maps from different convolution stages. Results at each stage from the

RGB image input and the gray-scaled depth map input are fused by a convolutional layer followed by a batch normalization layer. These fused features collectively yields the output from the backbone network. Then we feed the backbone outputs to a Feature Pyramid Network (FPN) [36] to fuse the features from different levels. On top of this extracted feature from the backbone network and the neck network, we attach Region Proposal Network (RPN) [51] and UOAISNet [2] as prediction heads for (1) amodal object bounding boxes, (2) visible object masks, (3) amodal object masks, and (4) occlusion predictions. An overview is shown in Figure 1.

Backbone Selection. We follow the work in [67] but adopt the pretrained ResNet-18 backbone instead of the more commonly used ResNet-50 backbone for the following two reasons: computation overhead and applicability of our theory. (1) As we are working with 7 loss functions and the gradient manipulation methods generally requires the gradient of each loss function w.r.t. the shared network parameters, which reside in the shallower layers, back propagation through the entire network has to be done for 7 times at each training iteration. The computation overhead will be even more if the backbone is deep, and especially when we are repeating each run for 3 times to make solid analyses. (2) The goal of this work is to investigate the behavior of existing MTL optimization algorithms in a real robotics application. Therefore, light-weighted networks would have more meaningful indications for real-world applications.

Training Objective and Baseline Definition. We attach supervision signals from foreground/background classification and bounding boxes regression to both the RPN head, yielding loss functions of $\mathcal{L}_{\text{rcls}}$ and $\mathcal{L}_{\text{rdet}}$, and to the amodal detection head, yielding \mathcal{L}_{cls} , and \mathcal{L}_{det} . Visible object masks prediction is supervised by \mathcal{L}_{vsb} and amodal object masks prediction is supervised by \mathcal{L}_{amd} . Finally, occluded-ness prediction is trained by minimizing \mathcal{L}_{occ} . We set our baseline to be trained by

$$\mathcal{L}_{\text{tot}} := \mathcal{L}_{\text{rcls}} + \mathcal{L}_{\text{rdet}} + \mathcal{L}_{\text{cls}} + \mathcal{L}_{\text{det}} + \mathcal{L}_{\text{vsb}} + \mathcal{L}_{\text{amd}} + \mathcal{L}_{\text{occ}}, \quad (4)$$

i.e., the sum of all 7 loss functions.

Hardware and Stability Considerations. Experiments are done on a pool of GPUs including NVIDIA RTX 6000 Ada Generation, NVIDIA RTX A6000, and NVIDIA GeForce RTX 4090. For stability consideration, we repeat each experiment run for at least 3 times and report the average of the evaluation metrics (Section 3) and also the trajectories of variables that we monitor during training (Section 5).

MTL Optimization Algorithms. We have conducted experiments with the following algorithms: 8 methods, PC-Grad [72], GradVac [66], GradDrop [6], RGW [35], MGDA [54], CAGrad [38], Nash-MTL [46], and Aligned-MTL [55], from the gradient manipulation category; 6 methods,

	BBox mAP	BBox mAR	VMask mAP	VMask mAR	AMask mAP	AMask mAR
Baseline	0.383	0.519	0.518	0.647	0.490	0.617
PCGrad [72]	0.370 (↓)	0.526 (↑)	0.500 (↓)	0.657 (↑)	0.454 (↓)	0.595 (↓)
GradVac [66]	0.393 (↑)	0.560 (↑)	0.521 (–)	0.680 (↑)	0.495 (–)	0.654 (↑)
GradDrop [6]	0.399 (↑)	0.541 (↑)	0.533 (↑)	0.666 (↑)	0.505 (↑)	0.634 (↑)
RGW [35]	0.358 (↓)	0.513 (↓)	0.490 (↓)	0.644 (–)	0.462 (↓)	0.614 (–)
MGDA [54]	0.371 (↓)	0.531 (↑)	0.452 (↓)	0.594 (↓)	0.430 (↓)	0.564 (↓)
CAGrad [38]	0.411 (↑)	0.557 (↑)	0.522 (–)	0.648 (–)	0.488 (–)	0.604 (↓)
Aligned-MTL [55]	0.400 (↑)	0.547 (↑)	0.477 (↓)	0.610 (↓)	0.460 (↓)	0.580 (↓)
IMTL [40]	0.410 (↑)	0.534 (↑)	0.550 (↑)	0.667 (↑)	0.541 (↑)	0.658 (↑)
CosReg [59]	0.387 (–)	0.545 (↑)	0.522 (–)	0.672 (↑)	0.488 (–)	0.631 (↑)
Uncertainty [30]	0.206 (↓)	0.349 (↓)	0.345 (↓)	0.507 (↓)	0.319 (↓)	0.482 (↓)
RLW [35]	0.360 (↓)	0.504 (↓)	0.499 (↓)	0.649 (–)	0.466 (↓)	0.614 (–)
FAMO [39]	0.431 (↑)	0.564 (↑)	0.517 (–)	0.623 (↓)	0.510 (↑)	0.613 (–)
DWA [41]	0.390 (↑)	0.533 (↑)	0.533 (↑)	0.664 (↑)	0.499 (↑)	0.628 (↑)
(rep) PCGrad	0.365 (↓)	0.522 (–)	0.504 (↓)	0.656 (↑)	0.468 (↓)	0.613 (–)
(rep) GradVac	0.338 (↓)	0.516 (–)	0.463 (↓)	0.628 (↓)	0.425 (↓)	0.585 (↓)
(rep) RGW	0.335 (↓)	0.494 (↓)	0.456 (↓)	0.617 (↓)	0.435 (↓)	0.593 (↓)
(rep) MGDA	0.423 (↑)	0.567 (↑)	0.533 (↑)	0.665 (↑)	0.515 (↑)	0.643 (↑)
(rep) CAGrad	0.408 (↑)	0.541 (↑)	0.538 (↑)	0.665 (↑)	0.513 (↑)	0.633 (↑)
(rep) Aligned-MTL	0.410 (↑)	0.554 (↑)	0.516 (–)	0.646 (–)	0.498 (↑)	0.625 (↑)
(rep) IMTL	0.380 (–)	0.526 (↑)	0.504 (↓)	0.656 (↑)	0.497 (↑)	0.651 (↑)
(rep) CosReg	0.387 (↑)	0.532 (↑)	0.530 (↑)	0.674 (↑)	0.492 (–)	0.629 (↑)

Table 1. Benchmark results of all selected methods with ResNet-18 backbone. Methods ran with feature-level gradients are marked by “(rep)”. Performance increase (with \uparrow) or decrease (with \downarrow) that’s more than 0.01 are shown in brackets after each table entry. Scores within 0.01 offset from the baseline are treated as comparable performance and labeled by “–”. Best viewed in color.

Uncertainty [30], GradNorm [5], IMTL [40], FAMO [39], RLW [35], and DWA [41], from the gradient balancing category; and CosReg [59] from the gradient regularization category. Among these, all 8 methods from the gradient manipulation category, GradNorm and IMTL from the gradient balancing category, and CosReg utilize the gradients of each loss function. Hence experiments could be easily repeated for their feature-level gradients or parameter-level gradients counterparts. In this paper, we adopt the abbreviation of prepending “(rep)” to a method to represent that this method is run with feature-level gradients, and methods run with parameter-level gradients are not prepended with anything.

Experiment Results. We make a note that we observed extremely poor performance when benchmarking GradNorm [5] and Nash-MTL [46], and the feature-level gradient counterpart of GradDrop [6], which is what originally proposed. Results of all other selected methods are summarized in Table 1. We conclude that GradVac [66], GradDrop [6], IMTL [40], DWA [41], (rep) MGDA [54], (rep) CAGrad [38], and (rep) CosReg [59] achieved consistent performance gain compared to the baseline on all 6 evaluation metrics. On the other hand, GradVac [66], IMTL [40], and (rep) MGDA achieved top-three performance under a majority (≥ 3) of the metrics. Finally, we conclude that (rep) MGDA, or more commonly known as MGDA-UB

[54], is the best-performing method among the 13 methods run with parameter-level gradients and the 8 methods run with feature-level gradients.

4. Fast Approximation by Feature-Level Gradients

It has been a common technique to replace $\nabla_{\theta^{\text{sh}}} \mathcal{L}_i$ with $\nabla_{\mathcal{Z}} \mathcal{L}_i$ for reduced computation cost [28, 54, 55]. While it might be reasonable to do so due to chain rule and sub-additivity of norms [54, 55], other methods [46] has reported significant performance degrade with feature-level gradients in their method. To the best of our knowledge, there is no work addressing the generalizability of this approximation.

The Nash-MTL paper [46] presents a preliminary analysis on this surrogate scheme. Here we expand further and aim to derive some relations between the two types of gradients.

$$\langle Ma, Mb \rangle = \text{Tr}((Ma)^\top (Mb)) = \text{Tr}(M^\top Mba^\top) \quad (5a)$$

$$= \left[(M^\top M) \circ (a \otimes b) \right] \cdot \text{sum}() \quad (5b)$$

where \circ denotes element-wise product, \otimes denotes outer product, and $\cdot \text{sum}()$ denotes summation of all entries in the preceding tensor. This derivation shows a close rela-

	BBox mAP	BBox mAR	VMask mAP	VMask mAR	AMask mAP	AMask mAR
PCGrad [72]	-1.4%	-0.7%	0.7%	-0.2%	3.2%	3.0%
GradVac [66]	-13.9%	-7.8%	-11.2%	-7.6%	-14.2%	-10.6%
RGW [35]	-6.4%	-3.6%	-6.9%	-4.2%	-5.9%	-3.4%
MGDA [54]	14.3%	6.8%	17.8%	12.0%	19.8%	14.1%
CAGrad [38]	-0.9%	-2.9%	2.9%	2.6%	5.1%	4.8%
Aligned-MTL [55]	2.5%	1.3%	8.1%	5.9%	8.3%	7.7%
IMTL [40]	-7.4%	-1.5%	-8.2%	-1.6%	-8.1%	-1.1%
CosReg [59]	0.2%	-2.3%	1.5%	0.3%	0.8%	-0.4%

Table 2. Benchmark results using ResNet-18 backbone but all gradients in the algorithms replaced with feature-level gradients. Table entries are relative performance change compared to their parameter-level gradient counterparts.

tionship between the inner products of the $\nabla_{\theta^{\text{sh}}} \mathcal{L}_i$'s and the outer products of the $\nabla_Z \mathcal{L}_i$'s, but not their inner products. Therefore, the angles in the θ^{sh} space does not translate directly to those in the Z space. On the other hand, for any matrix M and vector a , we have $\|Ma\|_2 \leq \|M\| \cdot \|a\|_2$. But the precise relative magnitude is not clear, yet. Hence, the validity of applying this proxy to algorithms like PCGrad [72], or reverting GradDrop [6] to its parameter-level gradient counterpart, is unclear.

In this section, we provide empirical results and answer the question of “how do the feature-level gradients counterpart compare with the parameter-level counterpart for each method, and whether this feature-level gradient surrogate work in general”. We compared the performance using $\nabla_{\theta^{\text{sh}}} \mathcal{L}_i$ versus $\nabla_Z \mathcal{L}_i$ on 8 optimization algorithms. The same results as in Table 1 were used but summarized as relative changes in Table 2. We address the following observations: (1) Only MGDA [54] and Aligned-MTL [55] achieved consistent performance gain under all evaluation metrics, and these are exactly the two selected methods that argued that feature-level gradients could be used as an upper bound (up to scaling) during the optimization process. (2) PCGrad [72], CAGrad [38], and CosReg [59] achieved comparable performance to their parameter-level counterparts. (3) GradVac [66], RGW [35], and IMTL [40] got significant performance degradation and hence this surrogate is clearly not applicable to these algorithms. Hence, the feature-level gradient surrogate cannot be generalized to all methods and whether it could be applied should be based on method-specific analyses and experiments.

5. Robust Analysis of Task Interference

In this section, we address the question of “whether task conflicts and task dominance are valid indicators for task interference” by monitoring gradient direction similarity (GDS) and gradient magnitude similarity (GMS) during training. This large-scale experiment results provides the community with valuable insights on the relationship between the optimization process and final performance. We

refer the readers to Section 6 for quantitative results.

We add evaluation proxies as optimizer hooks during training to monitor the changes in the level of task interference. Note that this monitoring process is expensive as, by definition, task interference should be measured by the gradients of each loss function w.r.t. the shared network parameters. This process also does not affect performance as these raw gradients are not accumulated or populated to the network parameters.

Throughout, we adopt the following notations: (1) for any vector v in some Euclidean space \mathbb{E} , $\|v\|_2$ will denote the ℓ_2 norm of v and (2) for any two vectors u and v in some Euclidean space \mathbb{E} , $\langle u, v \rangle$ will denote the inner product (dot product) of u and v .

5.1. Effect on Reducing Task Conflicts

We define the Gradient Direction Similarity (GDS) measure by

$$\alpha_{ij} := \frac{\langle \nabla_{\theta^{\text{sh}}} \mathcal{L}_i, \nabla_{\theta^{\text{sh}}} \mathcal{L}_j \rangle}{\|\nabla_{\theta^{\text{sh}}} \mathcal{L}_i\|_2 \|\nabla_{\theta^{\text{sh}}} \mathcal{L}_j\|_2} \text{ for } i, j \in [T]; \quad (6a)$$

$$\text{GDS} := \frac{1}{T(T-1)} \sum \left\{ \alpha_{ij} : i, j \in [T], i \neq j \right\}, \quad (6b)$$

where $\alpha_{ij} \in [-1, +1]$ is the cosine value of the angle between $\nabla_{\theta^{\text{sh}}} \mathcal{L}_i$ and $\nabla_{\theta^{\text{sh}}} \mathcal{L}_j$ and quantifies the relationship between the *directions* of the task gradients. This definition is widely adopted in the literature [59, 66, 72]. A lower GDS score indicates less agreement between the supervision from different losses. We train the model using the same scheme described in Section 3 and compute the GDS score every 10 iterations to monitor the change in task conflicts during the entire course of training. Visual results are shown in Figures 2 and 3. All curves are smoothed by taking the moving average with window size of 1/10 of the total trajectory length. The curves are plotted relative to those of the baseline method. For clarity, we added transparency to those not of interest and emphasized ones from which we make important observations.

We address the following 4 observations based on the GDS curves and Table 1: (1) Uncertainty [30], which had poor performance on the test set (Table 1), and GradVac [66], which had stronger performance, both achieved high GDS scores. (2) In contrast, PCGrad [72] and Aligned-MTL [55], which are hard to conclude one is superior to the other on the test set, lie far apart in the GDS plot. (3) For methods applied on feature-level gradients, (rep) PCGrad [72] and (rep) GradVac [66] had similar GDS scores, but it is clear from Table 1 that (rep) PCGrad performed better than (rep) GradVac under all metrics. (4) Moreover, (rep) MGDA and (rep) CosReg both showed strong performance on the test set but had their GDS curves appear far apart.

5.2. Effect on Reducing Task Dominance

We follow PCGrad [72] and define the Gradient Magnitude Similarity (GMS) as

$$\beta_{ij} := \frac{2\|\nabla_{\theta^{\text{sh}}} \mathcal{L}_i\|_2 \|\nabla_{\theta^{\text{sh}}} \mathcal{L}_j\|_2}{\|\nabla_{\theta^{\text{sh}}} \mathcal{L}_i\|_2^2 + \|\nabla_{\theta^{\text{sh}}} \mathcal{L}_j\|_2^2}, \text{ for } i, j \in [T]; \quad (7a)$$

$$\text{GMS} := \frac{1}{T(T-1)} \sum \left\{ \beta_{ij} : i, j \in [T], i \neq j \right\} \quad (7b)$$

where $\beta_{ij} \in [0, 1]$ quantifies the relationship between the *magnitudes* of the task gradients. A lower GMS score indicates less aligned learning pace between the losses. Visual results are shown in Figures 4 and 5.

We address 3 observations based on the GMS curves and Table 1: (1) MGDA [54] and FAMO [39] achieved almost the same GDS curves, but FAMO achieved significantly better performance results than MGDA. (2) For the feature-level gradient counterparts, (rep) MGDA and (rep) Aligned-MTL had almost the same GMS curves but (rep) MGDA performed clearly better than (rep) Aligned-MTL. (3) (rep) MGDA and (rep) IMTL curves reside on different sides of the curve for the baseline after the very early stage of training. However, (rep) MGDA was able to improve all metrics, and (rep) IMTL also achieved comparable performance to the baseline.

6. A Novel Perspective

We propose a novel perspective towards the challenges in MTL in real-world scenarios. Deep learning represents real-world information with data, encoding the data, and process and decode it back to human-interpretable form. With this vision, instead of putting our efforts on tackling the task interference problem during learning, we turn our attention to producing better latent spaces, i.e., learn more robust representations for the downstream tasks.

Single-task Learning (STL) is easy in the sense that each task could be solved independently. The gap between MTL and STL could be bridged by allocating disjoint subsets of

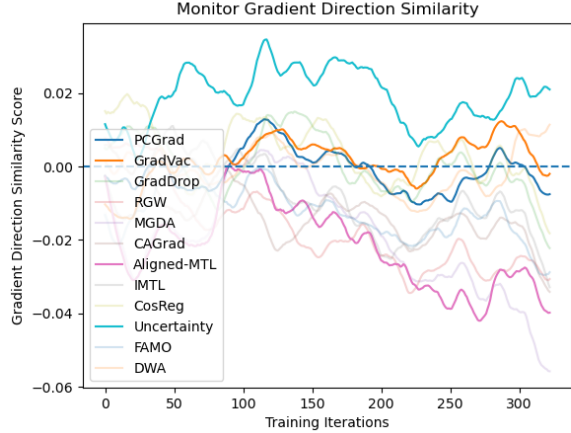


Figure 2. Training curves of GDS using gradients w.r.t. shared parameters.

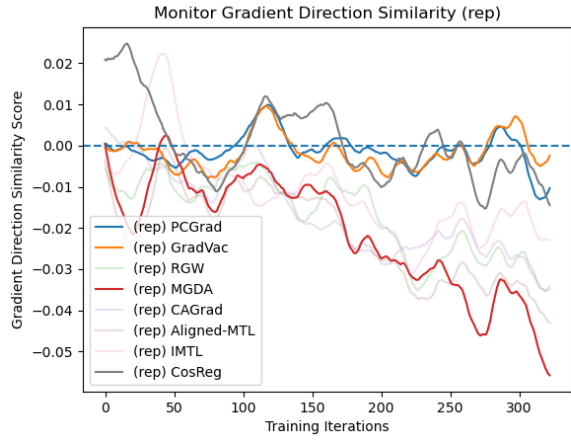


Figure 3. Training curves of GDS using gradients w.r.t. shared representation.

the extracted features for each task, while still using a single backbone. We propose to view the task interference problem from the feature disentanglement perspective. To the best of our knowledge, we are the first to explicitly measure the level of feature disentanglement and monitoring this quantity during training. We provide details in the following subsections.

6.1. Quantifying Feature Disentanglement

Given an extracted feature $\mathcal{Z} \in \mathbb{R}^d$ and individual task losses \mathcal{L}_i , how much a change in \mathcal{Z}_j can affect \mathcal{L}_i can be measured by $|\nabla_{\mathcal{Z}_j} \mathcal{L}_i| \in \mathbb{R}$. The tensor $|\nabla_{\mathcal{Z}} \mathcal{L}_i|$ of gradient magnitudes (element-wise absolute value), which has the same shape as \mathcal{Z} , can be interpreted as a saliency map. At location j , we can quantify the entropy of the saliencies

	BBox mAP	BBox mAR	VMask mAP	VMask mAR	AMask mAP	AMask mAR
GDS	0.643	0.633	0.505	0.600	0.567	0.510
GMS	0.676	0.705	0.538	0.595	0.505	0.590
FD	0.567	0.586	0.657	0.657	0.652	0.690

Table 3. Ranking similarity results for the three indicators gradient direction similarity (GDS), gradient magnitude similarity (GMS), and featur disentanglement (FD), and the 6 evaluation metrics. Similarity scores are converted to $[0.5, 1.0]$ as reversing the ordering yields a similarity score that is symmetric about 0.5.

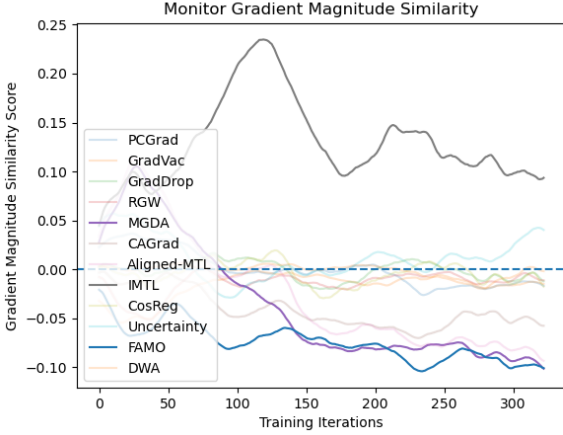


Figure 4. Training curves of GMS using gradients w.r.t. shared parameters.

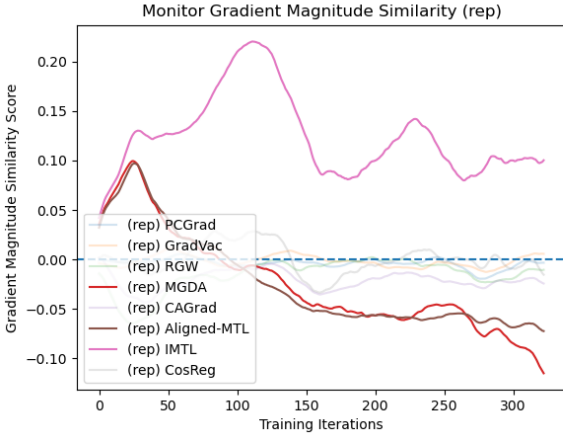


Figure 5. Training curves of GMS using gradients w.r.t. shared representation.

across all losses by

$$\mathcal{E}_j(\mathcal{Z}) := - \sum_{i=1}^T p_{ij} \log p_{ij}, \text{ where} \quad (8a)$$

$$p_{ij} := |\nabla_{\mathcal{Z}_j} \mathcal{L}_i| / \sum_{k=1}^T |\nabla_{\mathcal{Z}_j} \mathcal{L}_k| \quad (8b)$$

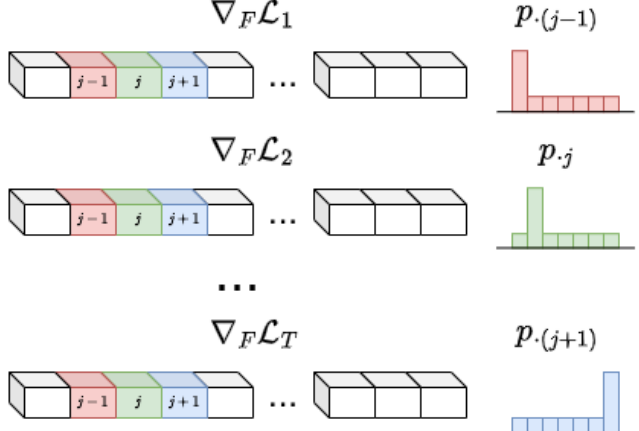


Figure 6. Illustration of feature disentanglement calculation. In the above, $p_{.j}$ denotes the mapping $i \mapsto p_{ij}$, which is the (smothened) distribution of feature saliency at location j across all tasks. Same for $p_{.(j-1)}$ and $p_{.(j+1)}$. If an extracted feature is entangled for the T down stream tasks, then each distribution $p_{.j}$ is concentrated at exactly one of the tasks i .

The entropy $\mathcal{E}(\mathcal{Z})$ for the entire feature tensor \mathcal{Z} can be simply defined to be the average entropy across all positions:

$$\mathcal{E}(\mathcal{Z}) := \frac{1}{d} \sum_{j=1}^d \mathcal{E}_j(\mathcal{Z}) \quad (9)$$

6.2. Monitoring Feature Disentanglement During Training

Following the same scheme as in Section 5, we also monitor feature disentanglement during training. Results are shown in Figures 7 and 8.

Most methods applied parameter-level gradients achieved feature entangle-ness lower than baseline close to the end of training, with the exception for RGW [35], PCGrad [72], MGDA [54], and Aligned-MTL [55]. These four methods form exactly the complement of the three methods that achieved performance gain among the gradient manipulation methods, as reported in Table 1. Nevertheless, clear decrease trends are displayed in PCGrad, MGDA, and Aligned-MTL.

When applied to feature-level gradients, all methods but

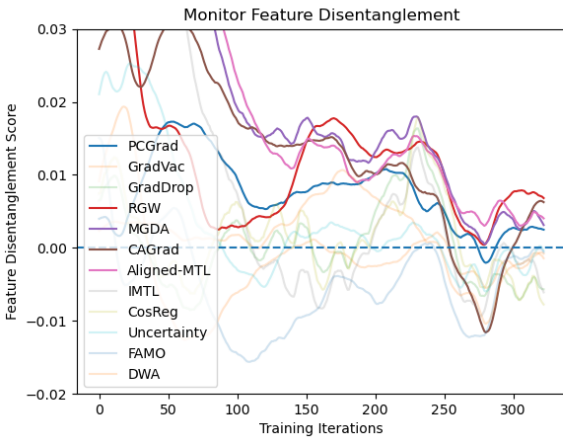


Figure 7. Training curves of GMS using gradients w.r.t. shared parameters.

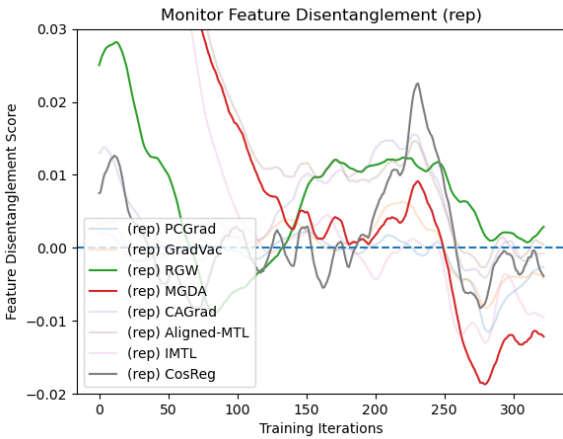


Figure 8. Training curves of GMS using gradients w.r.t. shared representation.

RGW achieved lower-than-baseline feature entangled-ness. This provides strong evidence that the previous success in these methods can be attributed to learning disentangled features for down stream tasks. Moreover, the existing methods can further disentangle the latent space when applied on feature-level gradients.

6.3. Ranking Similarity

In order to answer the question ‘‘whether task conflicts and task dominance, quantified by similarities in the directions and magnitudes of the gradients of each loss function and also the level of feature entanglement, are valid indicators of the phenomenon of task interference, which is the main drawback for MTL’’, we define Ranking Similarity and evaluate the alignment between these indicators during training

and the metrics during evaluation.

Definition. Given a set of scalars $A := \{a_1, \dots, a_n\} \subset \mathbb{R}$ and two rankings $R_1, R_2 : A \rightarrow [n]$, we define the similarity $\mathcal{S}(R_1, R_2)$ between R_1 and R_2 as the following average:

$$\frac{1}{n(n-1)} \sum_{\substack{i,j=1 \\ i \neq j}}^n \mathbb{I} \left[R_1 \text{ and } R_2 \text{ agree on } a_i \text{ and } a_j \right],$$

where for any $i, j \in [n]$ with $i \neq j$, R_1 and R_2 agree on a_i and a_j if and only if ‘‘ $R_1(a_i) > R_1(a_j)$ ’’ and ‘‘ $R_2(a_i) > R_2(a_j)$ ’’ have the same truth value. i.e., $\mathcal{S}(R_1, R_2)$ is the percentage of pairs (a_i, a_j) that has the same ordering under R_1 and R_2 .

When defining the ordering of training trajectories, we took the mean of the last 50 elements, which is the closest to the end of training. Results are shown in Table 3. We conclude that the FD measure is still reasonable on bounding box metrics but significantly and consistently higher on visible/amodal segmentation metrics.

6.4. Close Relation to GradDrop and CosReg

We address relation to GradDrop [6] and CosReg [59] in this subsection. In the original GradDrop [6] algorithm, we compute the gradients of the individual losses w.r.t. shared representation, and randomly let pass the positive or negative components. This approach is similar to disentangling the shared representation, but respecting only the gradient signs, not distribution of gradient magnitude. In the original CosReg algorithm, we penalize the gradients for not being orthogonal to each other. We can make a comparison by considering the feature-level counterpart. Gradients being orthogonal is a necessary but not sufficient condition for features being disentangled. Namely, only one component being close to zero would be sufficient for the cosine values to be small, but not the entropy.

7. Conclusions

We have showed that in the robotics grasping domain, GradVac [66], GradDrop [6], IMTL [40], DWA [41], and the feature-level gradients counterparts of MGDA [54], CAGrad [38], and CosReg [59], achieved consistent performance gain compared to the baseline. Among these, MGDA-UB [54] achieved the best performance. Comparing each method with parameter-level gradients versus feature-level gradients, we showed that only the methods MGDA [54] and Aligned-MTL [55] which have theoretical guarantees achieved a performance gain, while others were either similar or had significant performance degrade. We monitored the change in direction and magnitude similarities of the task gradients and showed that the rankings of the methods based on the GDS or GMS scores do not match well with those based on the final evaluation scores. We proposed ranking similarity and a novel perspective to monitor the training

process based on feature disentanglement scores, and showed that method ranking based on feature disentanglement clearly aligns better to those given by the test-set evaluation metrics on visible and amodal segmentation.

References

- [1] Milad Abdollahzadeh, Touba Malekzadeh, and Ngai-Man Man Cheung. Revisit multimodal meta-learning through the lens of multi-task learning. *Advances in Neural Information Processing Systems*, 34:14632–14644, 2021. [1](#)
- [2] Seunghyeok Back, Joosoon Lee, Taewon Kim, Sangjin Noh, Raeyoung Kang, Seongho Bak, and Kyobin Lee. Unseen object amodal instance segmentation via hierarchical occlusion modeling. In *2022 International Conference on Robotics and Automation (ICRA)*, pages 5085–5092. IEEE, 2022. [4](#)
- [3] Deblina Bhattacharjee, Tong Zhang, Sabine Süsstrunk, and Mathieu Salzmann. Mult: An end-to-end multitask learning transformer. In *Proceedings of the IEEE/CVF Conference on Computer Vision and Pattern Recognition*, pages 12031–12041, 2022. [4](#)
- [4] Tianlong Chen, Xuxi Chen, Xianzhi Du, Abdullah Rashwan, Fan Yang, Huizhong Chen, Zhangyang Wang, and Yeqing Li. Adamv-moe: Adaptive multi-task vision mixture-of-experts. In *Proceedings of the IEEE/CVF International Conference on Computer Vision*, pages 17346–17357, 2023. [4](#)
- [5] Zhao Chen, Vijay Badrinarayanan, Chen-Yu Lee, and Andrew Rabinovich. Gradnorm: Gradient normalization for adaptive loss balancing in deep multitask networks. In *International conference on machine learning*, pages 794–803. PMLR, 2018. [2, 3, 5](#)
- [6] Zhao Chen, Jiquan Ngiam, Yanping Huang, Thang Luong, Henrik Kretzschmar, Yunling Chai, and Dragomir Anguelov. Just pick a sign: Optimizing deep multitask models with gradient sign dropout. *Advances in Neural Information Processing Systems*, 33:2039–2050, 2020. [2, 4, 5, 6, 9](#)
- [7] Wonhyeok Choi and Sungsoon Im. Dynamic neural network for multi-task learning searching across diverse network topologies. In *Proceedings of the IEEE/CVF Conference on Computer Vision and Pattern Recognition*, pages 3779–3788, 2023. [4](#)
- [8] Jin-Dong Dong, An-Chieh Cheng, Da-Cheng Juan, Wei Wei, and Min Sun. Dpp-net: Device-aware progressive search for pareto-optimal neural architectures. In *Proceedings of the European Conference on Computer Vision (ECCV)*, pages 517–531, 2018. [4](#)
- [9] H. Drucker and Y. Le Cun. Double backpropagation increasing generalization performance. In *IJCNN-91-Seattle International Joint Conference on Neural Networks*, pages 145–150 vol.2, 1991. [3](#)
- [10] Kuo Du, Xiangbo Lin, Yi Sun, and Xiaohong Ma. Cross- infonet: Multi-task information sharing based hand pose estimation. In *Proceedings of the IEEE/CVF Conference on Computer Vision and Pattern Recognition*, pages 9896–9905, 2019. [4](#)
- [11] Nikita Dvornik, Konstantin Shmelkov, Julien Mairal, and Cordelia Schmid. Blitznet: A real-time deep network for scene understanding. In *Proceedings of the IEEE international conference on computer vision*, pages 4154–4162, 2017. [1, 4](#)
- [12] David Eigen and Rob Fergus. Predicting depth, surface normals and semantic labels with a common multi-scale convolutional architecture. In *Proceedings of the IEEE international conference on computer vision*, pages 2650–2658, 2015. [4](#)
- [13] Christopher Fifty, Ehsan Amid, Zhe Zhao, Tianhe Yu, Rohan Anil, and Chelsea Finn. Measuring and harnessing transference in multi-task learning. *arXiv preprint arXiv:2010.15413*, 2020. [2, 3](#)
- [14] Jörg Fliege and Benar Fux Svaiter. Steepest descent methods for multicriteria optimization. *Mathematical methods of operations research*, 51:479–494, 2000. [3](#)
- [15] Yuan Gao, Jiayi Ma, Mingbo Zhao, Wei Liu, and Alan L Yuille. Nddr-cnn: Layerwise feature fusing in multi-task cnns by neural discriminative dimensionality reduction. In *Proceedings of the IEEE/CVF conference on computer vision and pattern recognition*, pages 3205–3214, 2019. [4](#)
- [16] Yuan Gao, Haoping Bai, Zequn Jie, Jiayi Ma, Kui Jia, and Wei Liu. Mtl-nas: Task-agnostic neural architecture search towards general-purpose multi-task learning. In *Proceedings of the IEEE/CVF Conference on computer vision and pattern recognition*, pages 11543–11552, 2020. [4](#)
- [17] Maximilian Gilles, Yuhao Chen, Emily Zhixuan Zeng, Yifan Wu, Kai Furmans, Alexander Wong, and Rania Rayyes. Metagraspnetv2: All-in-one dataset enabling fast and reliable robotic bin picking via object relationship reasoning and dexterous grasping. *IEEE Transactions on Automation Science and Engineering*, pages 1–19, 2023. [2](#)
- [18] Ross Girshick. Fast r-cnn. In *Proceedings of the IEEE international conference on computer vision*, pages 1440–1448, 2015. [1, 4](#)
- [19] Shixiang Gu and Luca Rigazio. Towards deep neural network architectures robust to adversarial examples. *arXiv preprint arXiv:1412.5068*, 2014. [3](#)
- [20] SHI Guangyuan, Qimai Li, Wenlong Zhang, Jiaxin Chen, and Xiao-Ming Wu. Recon: Reducing conflicting gradients from the root for multi-task learning. In *The Eleventh International Conference on Learning Representations*, 2022. [1, 4](#)
- [21] Michelle Guo, Albert Haque, De-An Huang, Serena Yeung, and Li Fei-Fei. Dynamic task prioritization for multitask learning. In *Proceedings of the European conference on computer vision (ECCV)*, pages 270–287, 2018. [3](#)
- [22] Pengsheng Guo, Chen-Yu Lee, and Daniel Ulbricht. Learning to branch for multi-task learning. In *International conference on machine learning*, pages 3854–3863. PMLR, 2020. [4](#)
- [23] Kaiming He, Xiangyu Zhang, Shaoqing Ren, and Jian Sun. Deep residual learning for image recognition. In *Proceedings of the IEEE conference on computer vision and pattern recognition*, pages 770–778, 2016. [4](#)
- [24] Kaiming He, Georgia Gkioxari, Piotr Dollár, and Ross Girshick. Mask r-cnn. In *Proceedings of the IEEE international*

conference on computer vision, pages 2961–2969, 2017. 1, 4

[25] Zhijian Huang, Sihao Lin, Guiyu Liu, Mukun Luo, Chao-
qiang Ye, Hang Xu, Xiaojun Chang, and Xiaodan Liang.
Fuller: Unified multi-modality multi-task 3d perception
via multi-level gradient calibration. In *Proceedings of the
IEEE/CVF International Conference on Computer Vision*,
pages 3502–3511, 2023. 1

[26] Geethu Miriam Jacob, Vishal Agarwal, and Björn Stenger.
Online knowledge distillation for multi-task learning. In *Proceedings of the IEEE/CVF Winter Conference on Applications of Computer Vision*, pages 2359–2368, 2023. 3, 4

[27] Daniel Jakubovitz and Raja Giryes. Improving dnn robustness to adversarial attacks using jacobian regularization. In *Proceedings of the European conference on computer vision (ECCV)*, pages 514–529, 2018. 3

[28] Adrián Javaloy and Isabel Valera. Rotograd: Gradient homogenization in multitask learning. *arXiv preprint arXiv:2103.02631*, 2021. 3, 5

[29] Brendan Jou and Shih-Fu Chang. Deep cross residual learning for multitask visual recognition. In *Proceedings of the 24th ACM international conference on Multimedia*, pages 998–1007, 2016. 4

[30] Alex Kendall, Yarin Gal, and Roberto Cipolla. Multi-task learning using uncertainty to weigh losses for scene geometry and semantics. In *Proceedings of the IEEE conference on computer vision and pattern recognition*, pages 7482–7491, 2018. 1, 2, 3, 5, 7

[31] Iasonas Kokkinos. Ubernet: Training a universal convolutional neural network for low-, mid-, and high-level vision using diverse datasets and limited memory. In *Proceedings of the IEEE conference on computer vision and pattern recognition*, pages 6129–6138, 2017. 1, 4

[32] M Kumar, Benjamin Packer, and Daphne Koller. Self-paced learning for latent variable models. *Advances in neural information processing systems*, 23, 2010. 2

[33] Changsheng Li, Junchi Yan, Fan Wei, Weishan Dong, Qing-
shan Liu, and Hongyuan Zha. Self-paced multi-task learning.
In *Proceedings of the AAAI conference on artificial intelligence*, 2017. 2

[34] Yiyi Liao, Sarath Kodagoda, Yue Wang, Lei Shi, and Yong
Liu. Understand scene categories by objects: A semantic
regularized scene classifier using convolutional neural net-
works. In *2016 IEEE international conference on robotics and
automation (ICRA)*, pages 2318–2325. IEEE, 2016. 4

[35] Baijiong Lin, Feiyang Ye, Yu Zhang, and Ivor W Tsang.
Reasonable effectiveness of random weighting: A litmus test
for multi-task learning. *arXiv preprint arXiv:2111.10603*,
2021. 2, 3, 4, 5, 6, 8

[36] Tsung-Yi Lin, Piotr Dollár, Ross Girshick, Kaiming He,
Bharath Hariharan, and Serge Belongie. Feature pyra-
mid networks for object detection. In *Proceedings of the
IEEE conference on computer vision and pattern recogni-
tion*, pages 2117–2125, 2017. 4

[37] Xi Lin, Hui-Ling Zhen, Zhenhua Li, Qing-Fu Zhang, and
Sam Kwong. Pareto multi-task learning. *Advances in neural
information processing systems*, 32, 2019. 2, 3

[38] Bo Liu, Xingchao Liu, Xiaojie Jin, Peter Stone, and Qiang
Liu. Conflict-averse gradient descent for multi-task learn-
ing. *Advances in Neural Information Processing Systems*,
34:18878–18890, 2021. 2, 3, 4, 5, 6, 9

[39] Bo Liu, Yihao Feng, Peter Stone, and Qiang Liu. Famo:
Fast adaptive multitask optimization. *arXiv preprint
arXiv:2306.03792*, 2023. 2, 3, 5, 7

[40] Liyang Liu, Yi Li, Zhanghui Kuang, J Xue, Yimin Chen,
Wenming Yang, Qingmin Liao, and Wayne Zhang. Towards
impartial multi-task learning. *iclr*, 2021. 2, 3, 5, 6, 9

[41] Shikun Liu, Edward Johns, and Andrew J Davison.
End-to-end multi-task learning with attention. In *Proceedings of
the IEEE/CVF conference on computer vision and pattern
recognition*, pages 1871–1880, 2019. 3, 4, 5, 9

[42] Yongxi Lu, Abhishek Kumar, Shuangfei Zhai, Yu Cheng,
Tara Javidi, and Rogerio Feris. Fully-adaptive feature shar-
ing in multi-task networks with applications in person at-
tribute classification. In *Proceedings of the IEEE conference
on computer vision and pattern recognition*, pages 5334–
5343, 2017. 4

[43] Kevis-Kokitsi Maninis, Ilija Radosavovic, and Iasonas
Kokkinos. Attentive single-tasking of multiple tasks. In *Pro-
ceedings of the IEEE/CVF conference on computer vision
and pattern recognition*, pages 1851–1860, 2019. 4

[44] Ishan Misra, Abhinav Shrivastava, Abhinav Gupta, and Mar-
tial Hebert. Cross-stitch networks for multi-task learning. In
*Proceedings of the IEEE conference on computer vision and
pattern recognition*, pages 3994–4003, 2016. 4

[45] Eslam Mohamed and Ahmad El Sallab. Spatio-temporal
multi-task learning transformer for joint moving object de-
tection and segmentation. In *2021 IEEE International In-
telligent Transportation Systems Conference (ITSC)*, pages
1470–1475. IEEE, 2021. 4

[46] Aviv Navon, Aviv Shamsian, Idan Achituv, Haggai Maron,
Kenji Kawaguchi, Gal Chechik, and Ethan Fetaya. Multi-
task learning as a bargaining game. *arXiv preprint
arXiv:2202.01017*, 2022. 2, 3, 4, 5

[47] Davy Neven, Bert De Brabandere, Stamatios Georgoulis,
Marc Proesmans, and Luc Van Gool. Fast scene un-
derstanding for autonomous driving. *arXiv preprint
arXiv:1708.02550*, 2017. 1, 4

[48] Lerrel Pinto and Abhinav Gupta. Learning to push by grasp-
ing: Using multiple tasks for effective learning. In *2017
IEEE international conference on robotics and automation
(ICRA)*, pages 2161–2168. IEEE, 2017. 1

[49] Rajeev Ranjan, Vishal M Patel, and Rama Chellappa.
Hy-
perface: A deep multi-task learning framework for face de-
tection, landmark localization, pose estimation, and gender
recognition. *IEEE transactions on pattern analysis and ma-
chine intelligence*, 41(1):121–135, 2017. 4

[50] Dripta S Raychaudhuri, Yumin Suh, Samuel Schulter, Xiang
Yu, Masoud Faraki, Amit K Roy-Chowdhury, and Manmo-
han Chandraker. Controllable dynamic multi-task architec-
tures. In *Proceedings of the IEEE/CVF Conference on Com-
puter Vision and Pattern Recognition*, pages 10955–10964,
2022. 4

[51] Shaoqing Ren, Kaiming He, Ross Girshick, and Jian Sun.
Faster r-cnn: Towards real-time object detection with region

proposal networks. *Advances in neural information processing systems*, 28, 2015. 4

[52] Sebastian Ruder. An overview of multi-task learning in deep neural networks. *arXiv preprint arXiv:1706.05098*, 2017. 1

[53] Sebastian Ruder, Joachim Bingel, Isabelle Augenstein, and Anders Søgaard. Latent multi-task architecture learning. In *Proceedings of the AAAI Conference on Artificial Intelligence*, pages 4822–4829, 2019. 4

[54] Ozan Sener and Vladlen Koltun. Multi-task learning as multi-objective optimization. *Advances in neural information processing systems*, 31, 2018. 1, 2, 3, 4, 5, 6, 7, 8, 9

[55] Dmitry Senushkin, Nikolay Patakin, Arseny Kuznetsov, and Anton Konushin. Independent component alignment for multi-task learning. In *Proceedings of the IEEE/CVF Conference on Computer Vision and Pattern Recognition*, pages 20083–20093, 2023. 1, 2, 3, 4, 5, 6, 7, 8, 9

[56] Pierre Sermanet, David Eigen, Xiang Zhang, Michaël Mathieu, Rob Fergus, and Yann LeCun. Overfeat: Integrated recognition, localization and detection using convolutional networks. *arXiv preprint arXiv:1312.6229*, 2013. 1, 4

[57] Jure Sokolić, Raja Giryes, Guillermo Sapiro, and Miguel RD Rodrigues. Robust large margin deep neural networks. *IEEE Transactions on Signal Processing*, 65(16):4265–4280, 2017. 3

[58] Ximeng Sun, Rameswar Panda, Rogerio Feris, and Kate Saenko. Adashare: Learning what to share for efficient deep multi-task learning. *Advances in Neural Information Processing Systems*, 33:8728–8740, 2020. 4

[59] Mihai Suteu and Yike Guo. Regularizing deep multi-task networks using orthogonal gradients. *arXiv preprint arXiv:1912.06844*, 2019. 2, 3, 5, 6, 9

[60] Marvin Teichmann, Michael Weber, Marius Zoellner, Roberto Cipolla, and Raquel Urtasun. Multinet: Real-time joint semantic reasoning for autonomous driving. In *2018 IEEE intelligent vehicles symposium (IV)*, pages 1013–1020. IEEE, 2018. 4

[61] Jonas Uhrig, Marius Cordts, Uwe Franke, and Thomas Brox. Pixel-level encoding and depth layering for instance-level semantic labeling. In *Pattern Recognition: 38th German Conference, GCPR 2016, Hannover, Germany, September 12–15, 2016, Proceedings 38*, pages 14–25. Springer, 2016. 4

[62] Simon Vandenhende, Stamatios Georgoulis, Bert De Brabandere, and Luc Van Gool. Branched multi-task networks: deciding what layers to share. *arXiv preprint arXiv:1904.02920*, 2019. 4

[63] Simon Vandenhende, Stamatios Georgoulis, and Luc Van Gool. Mti-net: Multi-scale task interaction networks for multi-task learning. In *Computer Vision–ECCV 2020: 16th European Conference, Glasgow, UK, August 23–28, 2020, Proceedings, Part IV 16*, pages 527–543. Springer, 2020. 4

[64] Dániel Varga, Adrián Csiszárík, and Zsolt Zombori. Gradient regularization improves accuracy of discriminative models. *arXiv preprint arXiv:1712.09936*, 2017. 3

[65] Zirui Wang, Zachary C Lipton, and Yulia Tsvetkov. On negative interference in multilingual models: Findings and a meta-learning treatment. *arXiv preprint arXiv:2010.03017*, 2020. 1

[66] Zirui Wang, Yulia Tsvetkov, Orhan Firat, and Yuan Cao. Gradient vaccine: Investigating and improving multi-task optimization in massively multilingual models. *arXiv preprint arXiv:2010.05874*, 2020. 1, 2, 4, 5, 6, 7, 9

[67] Alexander Wong, Yifan Wu, Saad Abbasi, Saejith Nair, Yuhao Chen, and Mohammad Javad Shafiee. Fast grapsnext: A fast self-attention neural network architecture for multi-task learning in computer vision tasks for robotic grasping on the edge. In *Proceedings of the IEEE/CVF Conference on Computer Vision and Pattern Recognition*, pages 2292–2296, 2023. 4

[68] Dan Xu, Wanli Ouyang, Xiaogang Wang, and Nicu Sebe. Pad-net: Multi-tasks guided prediction-and-distillation network for simultaneous depth estimation and scene parsing. In *Proceedings of the IEEE Conference on Computer Vision and Pattern Recognition*, pages 675–684, 2018. 1, 4

[69] Yangyang Xu, Yibo Yang, and Lefei Zhang. Multi-task learning with knowledge distillation for dense prediction. In *Proceedings of the IEEE/CVF International Conference on Computer Vision*, pages 21550–21559, 2023. 4

[70] Yongxin Yang and Timothy M Hospedales. Trace norm regularised deep multi-task learning. *arXiv preprint arXiv:1606.04038*, 2016. 4

[71] Hanrong Ye and Dan Xu. Taskexpert: Dynamically assembling multi-task representations with memorial mixture-of-experts. In *Proceedings of the IEEE/CVF International Conference on Computer Vision*, pages 21828–21837, 2023. 4

[72] Tianhe Yu, Saurabh Kumar, Abhishek Gupta, Sergey Levine, Karol Hausman, and Chelsea Finn. Gradient surgery for multi-task learning. *Advances in Neural Information Processing Systems*, 33:5824–5836, 2020. 2, 4, 5, 6, 7, 8

[73] Hayoung Yun and Hanjoo Cho. Achievement-based training progress balancing for multi-task learning. In *Proceedings of the IEEE/CVF International Conference on Computer Vision*, pages 16935–16944, 2023. 2, 3

[74] Zhenyu Zhang, Zhen Cui, Chunyan Xu, Zequn Jie, Xiang Li, and Jian Yang. Joint task-recursive learning for semantic segmentation and depth estimation. In *Proceedings of the European Conference on Computer Vision (ECCV)*, pages 235–251, 2018. 4

[75] Zhenyu Zhang, Zhen Cui, Chunyan Xu, Yan Yan, Nicu Sebe, and Jian Yang. Pattern-affinitive propagation across depth, surface normal and semantic segmentation. In *Proceedings of the IEEE/CVF conference on computer vision and pattern recognition*, pages 4106–4115, 2019.

[76] Xiangyun Zhao, Haoxiang Li, Xiaohui Shen, Xiaodan Liang, and Ying Wu. A modulation module for multi-task learning with applications in image retrieval. In *Proceedings of the European Conference on Computer Vision (ECCV)*, pages 401–416, 2018. 1, 4